A Novel Analytic Method for the Broadband Determination of Electromagnetic Impedances and Material Parameters

Rolf Pelster

Abstract—**A simple analytic technique is described that allows the determination of complex impedances from quasistatic frequencies (some Hz) up to 2 GHz with one setup and a single sweep. Samples are placed in a shielded capacitor-like measurement cell that is inserted into a transmission line. The transmission coefficient of the setup is measured for one signal direction, i.e., only two receiver channels are needed. A complete calibration is achieved with only two standards. Dielectric and, with restrictions in the frequency range, magnetic material parameters can be determined via these impedance measurements. Temperature-dependent calibration and measurement are possible and even low losses down to $\tan\delta = 5 \cdot 10^{-4}$ and small impedances $Z \geq 0.05\ \Omega$ can be determined. The applicability of the method is experimentally verified over a frequency range of nearly nine decades from 5 Hz to 2 GHz.**

I. Introduction

In order to measure the impedance of an electronic component or the complex permittivity $\varepsilon = \varepsilon_1 - i\varepsilon_2$ and permeability $\mu = \mu_1 - i\mu_2$ of a material, precise broadband techniques are needed that should also allow to vary the temperature. Besides the low frequencies, the range between 1 MHz and 1 GHz is of special interest. Since the clock rates of PC's already lie above 10 MHz and are still increasing, the dielectric material of computer boards should be characterized up to 1 GHz. Absorber materials for anechoic chambers have to be tested above 10 MHz.

Until now, there has been no precise technique for the determination of complex impedances $Z = Z_1 + iZ_2$ that works in the low frequency range from 0–1 MHz as well as in the microwave region of a few GHz. Therefore, one has to use different techniques for a broadband characterization, requiring a lot of time and equipment.

Low-frequency techniques (e.g., balancing a bridge [1] or four-wire measurements) do not take into account phase variations and multiple reflections, and therefore precise measurements can be carried out only up to about 1 MHz. Time-domain methods do not allow complete error correction (calibration) and exhibit a lower accuracy and resolution at high frequencies.

Above 1 MHz, combined reflection and transmission measurements can be used requiring a more sophisticated setup (network analyzers). In general, a matched measurement cell with the unknown impedance is inserted into a transmission line. The influence of cables and instruments is taken into account using a three-step procedure, the calibration (for an overview see [2]), in which the measurement cell is replaced by three different standards. The reflection and transmission coefficients of each standard are measured for either possible signal directions, i.e., four complex values per measurement frequency and calibration standard. In addition to the time and equipment needed (bridges to split off reflected signals, reversal of signal direction) there are two principal disadvantages of these techniques that limit their application and accuracy. The used standards, e.g., a matched 50-Ω termination, change their properties as a function of temperature in an unknown way, so that high-precision measurements are possible only near room temperature. The same holds for pure reflection measurements, e.g., with a sample used as a termination of a coaxial line [3]. These techniques are not applicable below 1 MHz and they do not allow to measure highly conductive samples or to resolve loss tangents $\varepsilon_2/\varepsilon_1$ with values smaller than 10^{-1}, in an ideal case smaller than 10^{-2} (see e.g., [4]). A review about techniques for the determination of material parameters is given in [5] where also monochromatic methods (resonators) are discussed.

In this work a novel broadband transmission method for the determination of complex electromagnetic impedances is presented combining the simplicity of handling known from low-frequency techniques with the requirements at higher frequencies [6], [7]. It allows to determine complex electromagnetic impedances, e.g., passive electronic components (capacitors, inductances or resistors), from quasistatic frequencies up to 2 GHz using a single experimental setup. The complex permittivity and, with restrictions in the frequency range, the magnetic permeability of materials can be determined via these impedance measurements. Complete analytic calibration is achieved by measuring two simple known impedances. Because of the simplicity of the standards, temperature-dependent calibrations and measurements are possible.

II. Calibration and Impedance Measurement

Consider a measurement cell that is inserted into a transmission line [see Fig. 1(a)], i.e., it is connected to a signal source and the detector of a network analyzer or of a vector-voltmeter that automatically measures amplitude and phase of the transmission coefficient $S_{21}^{\text{meas}}(\nu)$. Between the electrodes

Manuscript received August 19, 1994; revised December 19, 1994. This work was supported by the Deutsche Forschungsgemeinschaft, Bonn (SFB 341/A3), and the Bundesministerium für Forschung und Technologie, Bonn (03M 2737B).

The author is with II. Physikalisches Institut der Universität zu Köln, 50937 Köln, Germany.

IEEE Log Number 9412051.

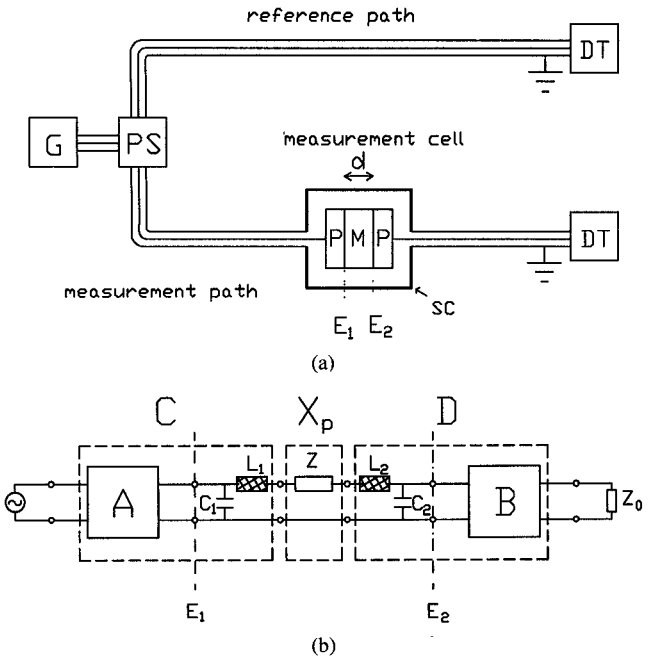

Fig. 1. Schematic view of the measurement system: (a) Capacitor inserted into a transmission line. G: power source, PS: power splitter, DT: detectors of reference and measurement path, P: condensor plates, M: sample of an unknown material, SC: shielding cover. (b) Equivalent circuit.

P (circular capacitor plates of radius r_c) there is a sample of a material M or an electronic component (radius $r \leq r_c$, length d). As will be pointed out, the specific form of the measurement cell and of the electrodes is not critical for the impedance measurement. However, a shielded parallel-plate capacitor is advantageous for the determination of the permittivity of a material. Since the transmission coefficients of the measurement and reference path are given by the complex voltage ratios of output and input, U_m/U_{in} and $U_{\text{ref}}/U_{\text{in}}$, the measured transmission coefficient $S_{21}^{\text{meas}} = U_m/U_{\text{ref}}$ represents just a normalization. Thus it is sufficient to consider only the generalized equivalent circuit of the measurement path [see Fig. 1(b)]. The complex cascading (or transmission) matrices A and B describe the transmission line up to the surfaces of the electrodes, which are located in the reference planes E_1 and E_2, respectively. They relate the incoming (a_i) and outgoing (b_i) signals of both sides of the corresponding two ports [8]: $(b_1, a_1) = A \cdot (a_2, b_2)$. The unknown impedance of the capacitor, Z, is given by the impedance of the sample and potential parallel capacitances and inductances (if the sample cross-section is smaller than the plates; see Section IV). L_1 and L_2 are self-inductances of the arrangement in the region between E_1 and E_2; C_1 and C_2 are capacitances between the cylindrical shielding cover of the measurement cell (SC) and the sample or the edges of the electrode surfaces. They depend on the geometry of the measurement cell and the plate distance d and determine the phase length of the transmission line between E_1 and E_2: $\phi = -\omega\sqrt{(L_1 + L_2)(C_1 + C_2)}$ (with $\omega = 2\,\pi\nu$). For our geometry and for a metallic sample ($Z = 0$) of length d this is just the phase length of a coaxial airline $\phi = \omega \cdot d/c$ (c: speed of light). In the frequency range in question ϕ can be assumed to be independent of the value of Z, i.e., of the actual sample radius $r \leq r_c$ (if smaller samples are measured) and the material properties provided the plate distance d is small compared to the distance between plates and shielding cover, $r_{\text{sh}} - r_c$ (we have chosen $r_{\text{sh}} = 15$ mm and $r_c = 6.5$ mm whereas in general $d \leq 1$ mm holds): The capacitances between the edges of the plates and the shielding cover (air gap measurement) roughly equal that of an coaxial airline [9], [10]. As long as $\omega|\Delta C| \cdot 2 \cdot Z_0 \ll 1$ holds (Z_0: termination impedance of the measurement path) the small changes of L_i and C_i for different samples will not influence the transmission coefficient (the same holds for the inductance as long as $\omega\Delta L/(2Z_0)$ll 1). Thus, the phase length ϕ is just given by the plate distance d and is independent of the value of Z.

Now the cascading matrices A and B may be extended to give a new simplified equivalent circuit. The impedance Z is connected in series between the two error two-ports described by the cascading matrices C and D. The cascading matrix of the whole system is obtained by multiplying those of the two-ports

$$T = C \cdot X_p \cdot D. \tag{1}$$

X_p being the cascading matrix of the two-port containing only the unknown impedance Z. Its corresponding reflection-(S_{ii}) and transmission-coefficients (S_{ij}) are $S_{11}^p = S_{22}^p = S_{21}^p \cdot Z/(2Z_0)$ and $S_{21}^p = S_{12}^p = (1 + Z/(2Z_0))^{-1}$ where Z_0 is the terminating impedance of the measurement branch. Therefore, X_p is given by

$$\begin{aligned} X_{11}^p &= -S_{11}S_{22}/S_{21} + S_{12} = 1 - Z/2Z_0 \\ X_{12}^p &= S_{11}/S_{21} = Z/2Z_0 \\ X_{21}^p &= -S_{22}/S_{21} = -Z/2Z_0 \\ X_{22}^p &= 1/S_{21} = 1 + Z/2Z_0 \end{aligned}$$

From (1) the measured transmission coefficient $S_{21}^{\text{meas}} = 1/T_{22}$ of the whole system is calculated yielding

$$S_{21}^{\text{meas}} = \frac{N}{KZ + 1} \tag{2}$$

with

$$\begin{aligned} N &= \frac{1}{C_{21}D_{12} + C_{22}D_{22}} \\ K &= \frac{N}{2Z_0} \cdot (-C_{21}D_{12} + C_{22}D_{22} + C_{21}D_{22} - C_{22}D_{12}) \end{aligned}.$$

N and K are functions of frequency, temperature (induced by thermal expansions of feeding lines and measurement cell) and of the plate distance d. They have to be determined by two additional transmission measurements, S_{21}^a and S_{21}^b—the so-called calibration. For this purpose Z is replaced by known impedances Z_a and Z_b, respectively.

In practice, different samples are investigated the lengths of which do not equal those of the used standards, d_a and d_b. Therefore, the resulting phase shift $\Delta\phi$ has to be taken into account. Equation (2) will be valid for Z_a and Z_b, if the respective transmission coefficient is replaced by

$$\begin{aligned} t_a &= S_{21}^a \exp\Big(i \cdot \frac{\omega}{c} \cdot (d_a - d)\Big) \\ t_b &= S_{21}^b \exp\Big(i \cdot \frac{\omega}{c} \cdot (d_b - d)\Big) \end{aligned}.$$

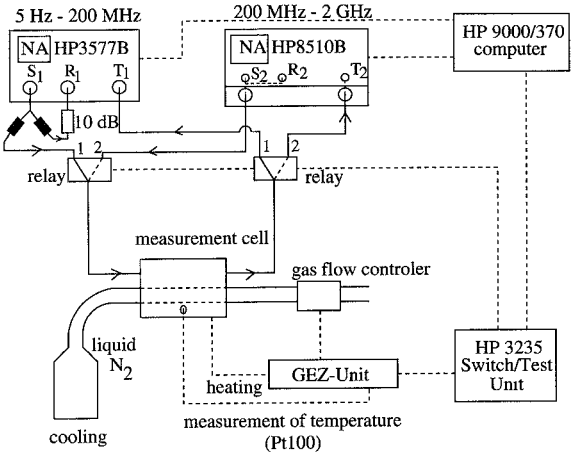

Fig. 2. Experimental setup for temperature controlled transmission measurements from 5 Hz to 2 GHz using two network-analyzers (see text). The HP 3235 Switch/Test Unit is used forthe remote control of the relay connection and for the temperature control.

Of course, the construction of the measurement cell has to ensure that a variation of the plate distance only changes the length of the transmission line between the reference planes E_1 and E_2. From (2) (for Z, Z_a and Z_b) the equation for the determination of Z is obtained

$$Z = \frac{Z_a t_a (t_b - S_{21}^{\text{meas}}) + Z_b t_b (S_{21}^{\text{meas}} - t_a)}{S_{21}^{\text{meas}} (t_b - t_a)}. \tag{3}$$

The measurement cell remains unchanged in the transmission path, only the impedances Z, Z_a and Z_b are exchanged. Thus, the reference planes of the calibration are the surfaces of the capacitor plates.

If the unknown impedance is connected parallel to Z_0, i.e., if it is connected between the inner conductor of the transmission path and ground, a similar calculation shows that the impedances in (3) have to be replaced by the respective admittances.

The maximum measurement frequency is determined by the geometry of the measurement cell. A first estimate can be made by considering capacitor plates, sample and cylindrical shielding cover as a part of a coaxial airline. For wavelengths $\lambda \leq \pi(r_c + r_{\text{sh}})$ higher modes, i.e., altered electromagnetic field distributions, become relevant in the region of the sample [9], [11]. These higher modes do not allow an unambigious determination of the impedance and thus

$$\nu_{\max} \leq \frac{c}{\pi(r_c + r_{\text{sh}})} \tag{4}$$

should hold. For $r_c = 6.5$ mm and $r_{\text{sh}} = 15$ mm, $\nu_{\max} \leq 4.4$ GHz. As we will show below, the experiments yield $\nu_{\max} \simeq 2$ GHz for this geometry.

The experimental setup is shown in Fig. 2. In order to cover the whole frequency range of the method two network-analyzers have been used for the measurement of the transmission coefficients (HP 3577B: 5 Hz-200 MHz/ HP 8510B: 200 MHz–2 GHz). They are connected to the measurement cell via two highly reproducible relay connections allowing computer-controlled measurements. Of course, the use of two analyzers is not a inherent feature of the method. Also, a single network-analyzer or a vector-voltmeter with an appropriate frequency range may be used. For temperature-dependent measurements from 100–450 K a hollow metallic cylinder surrounds the outer shielding cover of the measurement cell, which is cooled by liquid nitrogen and heated by a thermocoaxial cable.

III. Choice of Calibration Standards

The impedances Z_a and Z_b may be any known electronic components or materials between the electrodes. It is advantageous to choose a short $Z_a = 0$, i.e., a metallic ring with the outer diameter of the plates and a lossless, possibly unknown capacitance $C_b = 1/(i\omega Z_b)$ (air-gap or lossless spacer between the condenser-plates) as standards. With this choice (3) for the unknown inpedance $Z = Z_1 + iZ_2$ simplifies to

$$Z = \frac{t_a/S_{21}^{\text{meas}} - 1}{t_a/t_b - 1} \cdot \frac{1}{i\omega C_b}. \tag{5}$$

The value of C_b is real and independent of frequency, provided $\omega r_c/c < 0.3$ holds; this inequality corresponds to a maximum deviation of about 1% at the highest frequency [see [3], (11)], i.e., for a plate radius of $r_c = 6.5$ mm up to about 2 GHz. Since C_b is a real number, the loss tangent $\tan\delta = \varepsilon_2/\varepsilon_1 \simeq Z_1/Z_2$ [see (11)] is independent of its value and is exactly determined even if C_b is unknown. This is one reason for the high resolution of the method (see below).

The value of C_b may be determined directly from the measurements of S_{21}^a and S_{21}^b, if the measurements of the transmission coefficients are carried out over a larger frequency range containing also frequencies below 1 MHz. Below 1 MHz multiple reflections in the feeding lines are hardly noticeable [$C_{21}D_{12} \simeq C_{21}D_{22} \simeq C_{22}D_{12} \simeq 0$ and thus $K = 1/(2Z_0)$; see (2)]. Thus a simple normalizing procedure can be applied: $t_b = t_a/(1/(2Z_0 i\omega C_b) + 1)$. In general C_b is calculated in the frequency range near 500 kHz where the measured amplitude of t_b is sufficiently large, yielding a high measurement accuracy. A temperature dependent calibration is possible, because of the simplicity of the impedances (if the plate distance during the air gap measurement should depend on the temperature, C_b has to be calculated for each temperature point).

Equations (3) and (5) are independent of both the transmission line impedance Z_L and of the termination impedance Z_0, which may be unknown. Of course, at high frequencies above 500 kHz $Z_L = Z_0$ (in general 50 Ω) should hold to avoid unneccessary reflections caused by an impedance mismatch. The measured amplitudes of the transmission coefficients will be sufficiently large for both air gap and short. However, at low frequencies ($\nu \leq 500$ kHz) $|t_b/t_a| \simeq 2Z_0\omega C_b \ll 1$ [see (2)] holds and (5) becomes

$$Z \simeq \frac{t_b/S_{21}^{\text{meas}} - t_b/t_a}{i\omega C_b} \qquad \text{for } |t_b/t_a| \ll 1. \tag{6}$$

Therefore, the optimal calibration procedure should depend on $|Z|$ (Z_{dc} can be determined using a simple ohmmeter):

If $|Z|$ is small (in practice $|Z| \leq 20$ kΩ) residual nonlinearities of the detectors will become important because $|t_b| \ll |t_a|$ and $|t_b| \ll |S_{21}^{\text{meas}}|$ holds. Therefore, it is better to calculate Z

only from S_{21}^{meas} and t_a below 500 kHz using a normalizing procedure, i.e., $Z = 2\ Z_0(t_a/S_{21}^{\text{meas}} - 1)$.

For large $|Z|$ we have $|S_{21}^{\text{meas}}| \ll |t_a|$ and (6) further simplifies to $Z \simeq t_b/S_{21}^{\text{meas}} \cdot 1/(i\omega C_b)$. Thus the amplitude differences compared to t_a are not important. A normalizing procedure, however, would show the effects of nonlinearity and yield a lower resolution. Therefore, calibration with the second standard is necessary and (5) has to be used for all frequencies. In order to enhance the amplitude of the transmission coefficients and thus the measurement accuracy, a large termination impedance, e.g., $Z_0 = 1\ \text{M}\Omega$ (the exact value may be unknown), can be used below 500 kHz, while the termination impedance of the reference path remains unchanged (in general 50 Ω). This procedure is possible, for example, using modern network analyzers with programmable input impedances (see Fig. 2).

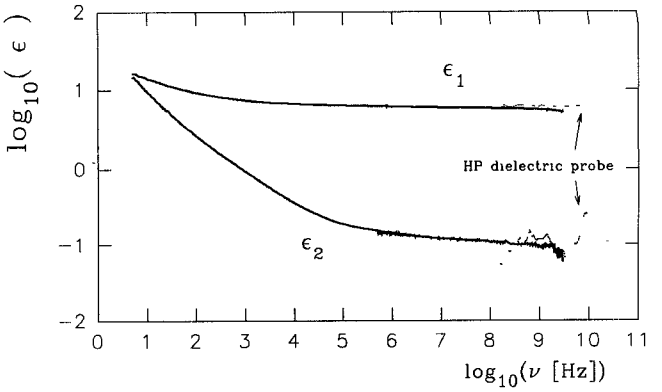

Fig. 3. Complex permittivity of an unsintered ceramic at room temperature versus frequency on a log.-log. plot. Solid line: method of this paper (5 Hz–3 GHz), dotted line: HP dielectric probe, an open coaxial reflection method (100 MHz–10 GHz).

IV. Calculation of the Impedance of the Sample

If the sample cross-section is smaller than the capacitor-plates an additional inductance and capacitance will contribute to the measured impedance Z. For example, liquid samples or powders may be filled in a cylindrical container with metallic front faces, which act as electrodes. Consider a cylindrically shaped sample of length d and radius $r \le r_c$ surrounded by a material (a container of inner diameter r, outer diameter r_c, permittivity ε_{sur}, and permeability μ_{sur}) or by air ($\varepsilon_{\text{sur}} = \mu_{\text{sur}} = 1$). From a calculation of the field distribution the impedance of the sample is obtained (see Appendix A)

$$Z_p = \frac{Z - i\omega L}{1 - i\omega(C_L + C_{\text{fr}})Z} \tag{7}$$

with

$$L = \frac{\mu_0\mu_{\text{sur}}}{2\pi} \cdot d \cdot \ln(r_c/r) \tag{8}$$

$$C_L = \varepsilon_0\varepsilon_{\text{sur}}\frac{\pi}{d} \cdot (r_c^2 - r^2). \tag{9}$$

(ε_0, μ_0: permittivity and permeability of vacuum). C_{fr} is the fringing capacitance between the edges of the two condensor plates. Since $r \le r_c$ its value is independent of the material between the plates. The inductance L takes into account the phase shift due to the smaller sample radius $r \le r_c$. At low frequencies $1 \gg \omega|L/Z|$ (7) becomes $1/Z = 1/Z_p + i\omega(C_L + C_{\text{fr}})$, i.e., a simple parallel circuit of sample and surrounding medium.

Since a capacitance C_b has been measured as a second calibration standard, the difference between its experimentally determined value (see Section III) and its theoretical value (neglecting the fringing fields) equals the fringing capacitance

$$C_{\text{fr}}(d_b) = C_b - \varepsilon_0\frac{A_e + (\varepsilon_b - 1)A_b}{d_b}$$

(A_e: area of the capacitor plates; A_b: area of a possible spacer of permittivity ε_b and thickness d_b). A direct theoretical calculation is difficult because of the influence of the surrounding shielding cover [9], [10]. In the case of different electrode distances, the fringing capacity for the measurement of a sample (thickness $d \ne d_b$) has to be corrected. In general this correction is much smaller than the capacitance of the sample. An approximative formula is given in Appendix B

$$C_{\text{fr}}(d) \simeq C_{\text{fr}}(d_b) + 2 \cdot \varepsilon_0 r_c \cdot \ln(d_b/d). \tag{10}$$

Of course, the highest accuracy is achieved for $d_b \simeq d$.

V. Determination of Mateal Parameters

The impedance of a cylindrically shaped sample is

$$Z_p = \frac{U_p}{I_p} = \frac{\int_0^{d_p} E(r)\,dz}{\oint H(r)\,dl} = \frac{E(r)d_p}{2\pi r H(r)}$$

where $E(r)$ and $H(r)$ are the axial electric and circumferential magnetic fields (see Appendix A)

$$E(r) = E_0 J_0(kr)\exp(-i\omega t)$$

$$H(r) = iE_0\sqrt{\frac{\varepsilon_0\varepsilon}{\mu_0\mu}}J_1(kr)\exp(-i\omega t)$$

($\varepsilon = \varepsilon_1 - i\varepsilon_2$: complex permittivity of the material; $\mu = \mu_1 - i\mu_2$: complex permeability of the material; $d_p = d - d_m$ length of the sample without thickness, d_m, of possible metallic contacts; $k = \frac{\omega}{c}\sqrt{\varepsilon\mu}$: complex wave vector; J_0, J_1: complex Bessel function of 0th and 1st order). Skin effects are taken into account via J_0 and J_1. Thus the complex permittivity is calculated from the capacitance $C_p = 1/(i\omega Z_p)$ by solving the equation

$$C_p = C_0 \cdot \varepsilon \cdot \frac{2J_1(kr)}{krJ_0(kr)} \tag{11}$$

(see also [3]), for example by a numerical search for zeros ($C_0 = \varepsilon_0\pi r^2/d_p$). At low frequencies ($|kr| \ll 1$), (11) becomes $C_p = C_0\varepsilon \cdot (1 + (kr)^2/8 + \cdots)$ and thus $\varepsilon = C_p/C_0$, which is the well-known low-frequency formula for plate capacitors. Then also samples with noncircular cross-sections may be investigated.

In Fig. 3 the result of a measurement on a unsintered ceramic is shown. In order to compare with a commercial reflection method (material as termination of an open coaxial cable, ν = 100 MHz–10 GHz) the front faces of the sample have not been metallized. The curve consist of about 1000

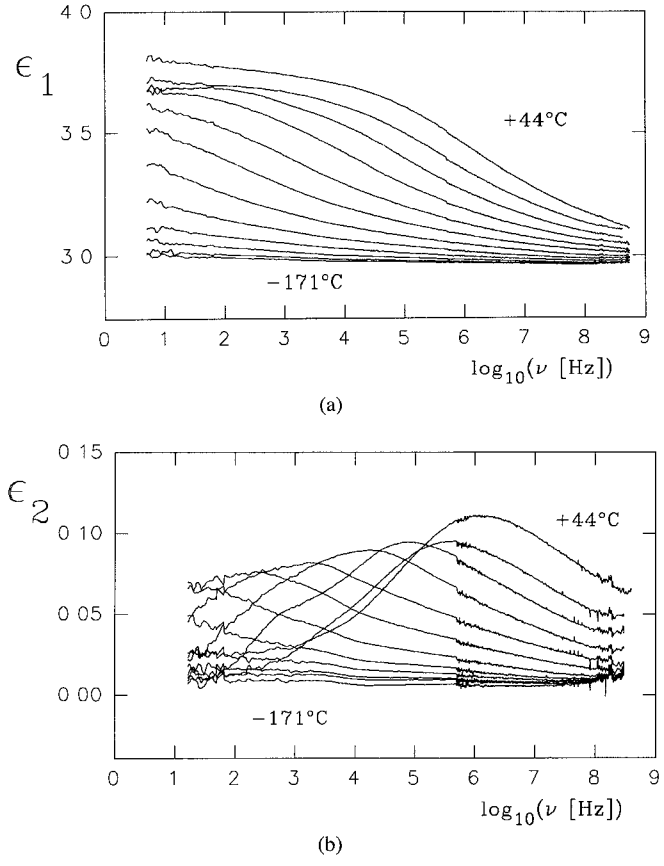

Fig. 4. Permittivity of PETG, an amorphous polymer, versus frequency at temperatures between 44°C and −171°C (from 44°C to −156°C in steps of 20°C) on a semi-log.plot. The imperfect sample geometry determines the upper frequency limit.

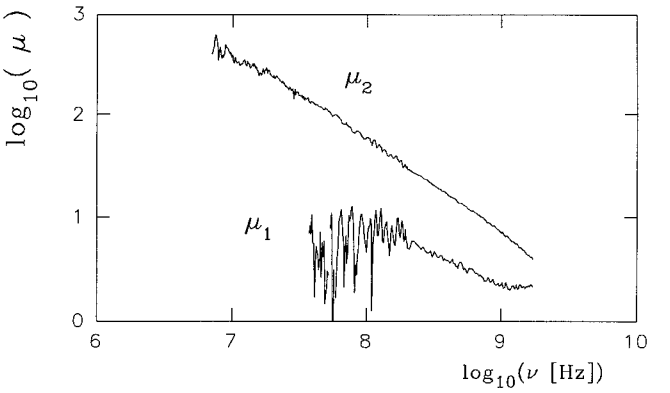

Fig. 5. Magnetic permeability $\mu = \mu_1 - \imath\mu_2$ versus frequency of a magnetic material (TDK IB-011) at room temperature on a log.-log. plot.

frequency points and no averaging or numerical smoothing has been applied. The extremely broad frequency range and the high resolution of the method can easily be observed while losses below $\varepsilon_2/\varepsilon_1 \simeq 5 \cdot 10^{-2}$ can hardly be resolved by the open coaxial reflection method (see Fig. 3). In [12] results are compared to waveguide measurements in the range of 10 GHz. Of course, conductive samples can also be studied. An example showing the large measurement range is given in [13], where insulating and conductive polymer blends (over 14 orders of magnitude, from $\sigma = \varepsilon_0\varepsilon_2\omega = 10^{-12}$ to 10^2 $\Omega^{-1}\mathrm{m}^{-1}$) have been investigated. Also temperature dependent calibration and measurement are possible (see Fig. 4).

At higher frequencies a considerable circumferential magnetic field exists between the plates and thus magnetic materials ($\mu = \mu_1 - \imath\mu_2 \neq 1$) may also be investigated. For $|kr| \not\ll 1$ two samples of different radii can be used to determine the independent quantities ε and μ. This yields two equations of the same form as (11), but for different radii r. Fig. 5 displays the permeability (above 10 MHz) of a magnetic material (TDK IB-011). Further results will be published later.

Equation (11) is derived under the assumption that the electric field between the capacitor plates is purely perpendicular to the plates, i.e., $|kd_p| < 1$ has to hold. In general it can be seen from the frequency dependence of the permittivity whether this limit has been exceeded. In order to rule out any influence of a disturbed field distribution $|kd_p| \leq 0.2$ is used. Thus the upper frequency limit for an accurate evaluation of the material parameters is $\nu \leq 0.2 \cdot c/(2\pi d_p\sqrt{|\varepsilon\mu|})$, i.e.,

$$\nu_{\max}[\mathrm{GHz}] \leq \frac{10}{\sqrt{|\varepsilon\mu|}\, d_p[\mathrm{mm}]}$$

or in the case of conductive samples $[\sigma_1/(\varepsilon_0\omega) = \varepsilon_2 \gg \varepsilon_1]$

$$\nu_{\max}[\mathrm{GHz}] \leq \frac{5}{\sigma_1[S/m] \cdot d_p^2[\mathrm{mm}^2] \cdot |\mu|}$$

Using thinner samples will therefore increase the maximum measurement frequency, which indicates the limit for the determination of ε. On the other hand very small electrode distances will result in large capacitances or small impedances. Thus at high frequencies the transmission coefficient may not sufficiently differ from that of a metallic short [see (2)] resulting in a smaller accuracy of the measurement (see below).

VI. Resolution and Accuracy

In this section we shall focus on the theoretical accuracy limits which are given by the uncertainty of the phase (φ) and amplitude (A) measurement. With modern network analyzers an accuracy up to $\Delta A/A = \Delta\varphi[\mathrm{rad}] = 2.5 \cdot 10^{-4}$ can be achieved after calibration, i.e., a reproducibility of 0.002 dB and 0.014°. Of course, an additional phase error $\Delta\varphi = \omega/c \cdot \Delta d$ (c: speed of light in vacuum) will occur at high frequencies, if the thickness of the sample and of its metallic contacts are not exactly known or if the corresponding front faces of the samples are not parallel! In order to avoid air gaps or contact resistances the front faces of samples should be metallized (air gaps caused by non-parallel front faces or by surface roughness would yield a too small measured permittivity; see [3]). In practice the relative error of the sample geometry $\Delta_{\mathrm{rel}}(r^2/d_p)$ has to be added to the error of $\Delta_{\mathrm{rel}}|\varepsilon| = \Delta|\varepsilon|/|\varepsilon|$ (in general $\Delta_{\mathrm{rel}}(r^2/d_p)$ is in the range of 1%). The loss tangent, however, is nearly geometry independent for $r \simeq r_c$.

Neglecting geometry deficiencies, $\Delta_{\mathrm{rel}}|Z_p| \simeq \Delta_{\mathrm{rel}}|\varepsilon|$ and $\Delta_{\mathrm{rel}}(Z_1/Z_2) \simeq \Delta_{\mathrm{rel}}(\varepsilon_2/\varepsilon_1)$ hold. In Appendix C the

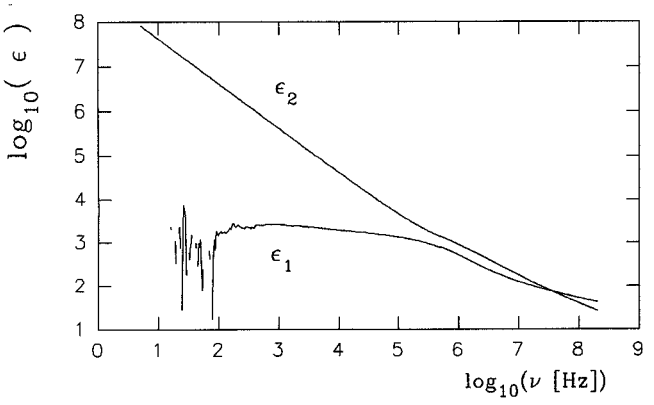

Fig. 6. Permittivity of a TiC/polymer composite at room temperature on a log.-log.plot.

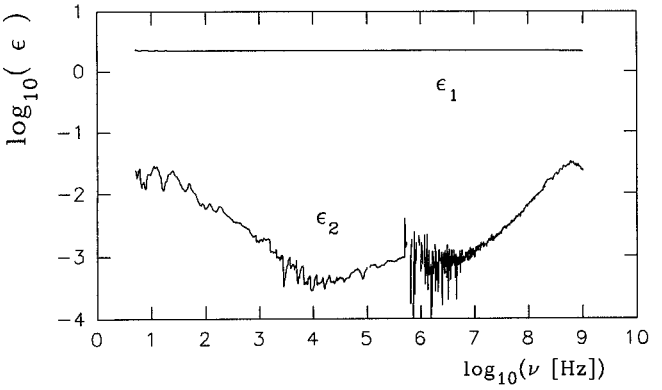

Fig. 7. Permittivity of polyethylene at room temperature on a log.-log.plot.

relative accuracy of measurement of a nonmagnetic sample with radius $r = r_c$ is shown to be [(15) and (16)]

$$\Delta_{\text{rel}}|\varepsilon| \simeq 5 \cdot 10^{-4} \cdot (1 + \alpha \cdot |\varepsilon|)$$

$$\Delta_{\text{rel}}\left(\frac{\varepsilon_2}{\varepsilon_1}\right) \simeq 5 \cdot 10^{-4} \cdot (1 + \alpha|\varepsilon|) \cdot \left(\frac{\varepsilon_1}{\varepsilon_2} + \frac{\varepsilon_2}{\varepsilon_1}\right)$$

with $\alpha = 2\ Z_0 \omega C_0$ [$C_0 = \varepsilon_0 \pi r_c^2/d_p$]. This accuracy corresponds to the reproducibility of measurements using the same sample. The range where the loss tangent $\tan\delta = \varepsilon_2/\varepsilon_1$ can be resolved is given by $\Delta_{\text{rel}}\left(\frac{\varepsilon_2}{\varepsilon_1}\right) = 1$ and thus

$$5 \cdot 10^{-4} \cdot (1 + \alpha|\varepsilon|) \leq \frac{\varepsilon_2}{\varepsilon_1} \leq \frac{2 \cdot 10^3}{1 + \alpha|\varepsilon|}.$$

For $\alpha \cdot |\varepsilon| < 0.1$ the accuracy is independent of frequency and the geometric error $\Delta_{\text{rel}}(r^2/d_p)$ will determine the accuracy of $\Delta_{\text{rel}}|\varepsilon|$. Fig 6 shows the permittivity of a conductive TiC/polymer composite. Below 100 Hz $\varepsilon_2/\varepsilon_1 > 10^3$ holds and the real part of ε cannot be resolved. In Fig. 7 the permittivity of a polyethylene sample is displayed. At 10 kHz a loss tangent of about $2 \cdot 10^{-4}$ is measured. At low frequencies the measurement amplitudes are small and thus the accuracy is decreased, as can be seen from the noise in ε_2. The same effect is observed near 500 kHz where the terminaton impedance of the network analyzer is switched from $Z_0 = 1$ MΩ to 50 Ω. In the case of large $|\varepsilon|$ or small sample thickness, the accuracy is decreased at high frequencies ($\alpha|\varepsilon| > 1$).

Since $\alpha|\varepsilon| \simeq 2Z_0/|Z_p|$ the smallest impedance which can be measured ($\Delta_{\text{rel}}|\varepsilon| = \Delta_{\text{rel}}|Z_p| = 1$) is $|Z_p|_{\min} = 2Z_0 \cdot 5{\cdot}10^{-4} = 0.05\ \Omega$.

VII. Conclusion

A novel broad-band calibration and measurement method for the investigation of materials (solids, compressed powders or liquids) and for passive electronic components has been presented and experimentally verified over a frequency range of nearly 9 decades from 5 Hz–2 GHz. A further miniaturization of the measurement cell would raise the upper frequency limit. The method exhibits several advantages:

1) Only transmission measurements in one signal direction are needed, i.e., detectors and bridges or directional couplers for the measurement of reflected signals are not necessary and two detectors are sufficient.
2) The influence of the transmission path and of the measurement cell are taken into account analytically by only two calibration measurements, i.e., there are no systematic errors in the determination of the impedance due to mathematical approximations.
3) Temperature-dependent calibration and measurements are possible because of the simplicity of the calibration standards.
4) The measurement cell that contains the unknown impedance does not have to match the line impedance. Therefore, a lot of different measurement cells may be used. By choosing an appropriate geometry of measurement cell and electrodes the effort for the preparation of suitable samples can be kept to a minimum. Also, other types of measurement cells with two electrodes can be used. For example, it would be possible to determine the complex inductance of a material-filled coil (calibration with a short and the unloaded coil).
5) The measurement range is very large, and the accuracy of the method is very high. Even very small impedances down to $|Z_p| = 0.05\ \Omega$ and impedances having a small loss tangent ($Z_1/Z_2 \simeq \varepsilon_2/\varepsilon_1 \simeq 5 \cdot 10^{-4}$) can be determined.

Appendix A
Field Distribution and Impedance of the Sample

In order to determine the impedance of a cylindrically shaped sample (radius $r \leq r_c$, thickness d, complex permittivity ε and complex permeability μ) between two circular capacitor-plates of radius r_c the field calculation of Kolodziej and Sobczyk [14] (coaxial sample holder for reflection measurements) is followed. However, the calculation differs at the transition from electric and magnetic field to the integrated values of voltage and current. Dissipation in the material is *a priori* taken into account, i.e., the restrictions given in [14] are not valid. In addition, the sample may be surrounded by a known material (a container of inner diameter r, outer diameter r_c, complex permittivity ε_{sur} and complex permeability

μ sur; for details see [6]). The solution of the wave equation yields an axial electric and a circumferential magnetic field

$$E = E_z = E_0 J_0(k_1 a) e^{-i\omega t} \qquad 0 \le a \le r$$
$$H = H_\phi = i \cdot E_0 / Z_1 \cdot J_1(k_1 a) e^{-i\omega t}$$

$$E = E_z = \rho_1 J_0(k_2 a) + \rho_2 N_0(k_2 a) \qquad r \le a \le r_c$$
$$H = H_\phi = i \cdot [\rho_1 J_1(k_2 a) + \rho_2 N_1(k_2 a)]/Z_2$$

(J_0, J_1: complex Bessel-function of 0th and 1st order; N_0, N_1: complex Neumann function of 0th and 1st order, ρ_1, ρ_2: complex constants; $k_1 = \omega/c \cdot \sqrt{\varepsilon\mu}$, $k_2 = \omega/c \cdot \sqrt{\varepsilon_{\text{sur}}\mu_{\text{sur}}}$: wave vectors of the sample and of the surrounding medium with corresponding wave impedances $Z_1 = \sqrt{\mu_0\mu/(\varepsilon_0\varepsilon)}$ and $Z_2 = \sqrt{\mu_0\mu_{\text{sur}}/(\varepsilon_0\varepsilon_{\text{sur}})}$.

In this calculation disturbed fields at the edges of the plates are neglected and the electrical field is assumed to be purely perpendicular to the plates and constant in the z-direction ($\partial E/\partial z \simeq 0$). The latter relation corresponds to $|k_1 d| < 1$ and $|k_2 d| < 1$. The continuity of the tangential fields at $a = r$ yields the complex constants

$$\rho_2 = \frac{J_0(x_1) \cdot [iZ_2 H(r) + E(r) J_1(x_1)/J_0(x_1)]}{N_0(x_1) J_1(x_1) - J_0(x_1) N_1(x_1)}$$
$$\rho_1 = \frac{E(r) - \rho_2 N_0(x_1)}{J_0(x_1)}$$

with $x_1 = k_2 r$ and $x_2 = k_2 r_c$. Thus the fields at $a = r_c$ are

$$E(r_c) = \beta E(r) + \alpha i Z_2 H(r)$$
$$H(r_c) = \frac{i}{Z_2} \cdot E(r)\delta - \gamma H(r)$$

with

$$\alpha = [J_0(x_1)N_0(x_2) - N_0(x_1)J_0(x_2)]/NE$$
$$\beta = [J_1(x_1)N_0(x_2) - N_1(x_1)J_0(x_2)]/NE$$
$$\gamma = [J_0(x_1)N_1(x_2) - N_0(x_1)J_1(x_2)]/NE.$$
$$\delta = [J_1(x_1)N_1(x_2) - N_1(x_1)J_1(x_2)]/NE$$
$$NE = J_1(x_1)N_0(x_1) - J_0(x_1)N_1(x_1)$$

In order to calculate the impedance of the capacitor the integrated fields have to be considered. The voltage $U = \int_0^d E(r_c)\,dz$ between the surfaces of the capacitor plates is

$$U = E(r_c)d = \beta E(r)d + \alpha i Z_2 \frac{d}{2\pi r} H(r) 2\pi r$$
$$= \beta U_p + \alpha i Z_2 \frac{d}{2\pi r} I_p. \qquad (12)$$

$U_p = \int_0^d E(r)\,dz$ and $I_p = \oint H(r)dl$ are the voltage across the sample and the current through the sample. The total current $I = \oint H(r_c)\,dl$ is

$$I = H(r_c)2\pi r_c = -\gamma 2\pi r H(r) \cdot \frac{r_c}{r} + i\delta \frac{2\pi r_c}{Z_2 d} \cdot E(r)d$$
$$= -\gamma I_p \cdot \frac{r_c}{r} + i\delta \frac{2\pi r_c}{Z_2 d} \cdot U_p. \qquad (13)$$

Equations (12) and (13) yield the impedance of the sample $Z_p = U_p/I_p$ as a function of the total measured impedance Z

$$Z_p = \frac{Z - i\omega L}{\eta - i\omega C_L Z} \qquad (14)$$

where η, the inductance L and the capacitance C_L are defined as follows:

$$L = \frac{-Z_2 d}{2\pi r_c \omega} \cdot \frac{\alpha}{\gamma}$$
$$C_L = \frac{-2\pi r}{Z_2 d \cdot \omega} \cdot \frac{\delta}{\gamma}.$$
$$\eta = \frac{-r}{r_c} \cdot \frac{\beta}{\gamma}$$

Substituting the Taylor series expansions of the Bessel- and Neumann-functions in α, β, γ and δ and neglecting terms of order x^2 yields (8) and (9) (see Section IV) and $\eta = 1$. For $r_c = 6.5$ mm, $r = 5$ mm, $\varepsilon_{\text{sur}} = \mu_{\text{sur}} = 1$, and $\nu = 2$ GHz the error due to this approximation is smaller than 1%. In order to take into account the fringing fields between the capacitor plates, C_L is replaced by $C_L + C_{\text{fr}}$ and thus (7) is obtained.

Appendix B
Correction of the Fringing Capacitance

In Section IV it has been pointed out how to determine the fringing capacitance $C_{\text{fr}}(d_b)$ between the two capacitor plates by experiment. Since the plate distance of calibration d_b and sample measurement d may differ, $C_{\text{fr}}(d)$ has to be calculated for an accurate evaluation of the permittivity. Consider first Kirchhoffs formula [15]

$$C_{\text{fr}}(d) = \varepsilon_0 r_c \left[\ln\left(\frac{16\pi r_c(d+w)}{d^2}\right) + \frac{w}{d} \cdot \ln\left(\frac{d+w}{w}\right) - 1\right]$$

for a capacitor without shielding cover (w: thickness of the plates) yielding for $\Delta C_{\text{fr}} = C_{\text{fr}}(d) - C_{\text{fr}}(d_b)$

$$\Delta C_{\text{fr}} = \varepsilon_0 r_c [2 \cdot \ln(d_b/d) + (1 + w/d) \cdot \ln(1 + d/w) - (1 + w/d_b) \cdot \ln(1 + d_b/w)]$$

If electrodes and sample are considered as a part of a coaxial airline, $w \gg d$, $w \gg d_b$ should hold rather independently of the actual thickness of the capacitor plates. A Taylor series expansion yields

$$\Delta C_{\text{fr}} = \varepsilon_0 r_c [2 \cdot \ln(d_b/d) - 1/2 \cdot (d_b - d)/w + \cdots]$$

and thus (10) of Section IV. This relation has been verified by experiment and is a good approximation even if the thickness of the sample exceeds that of the plates. Of course, the surrounding shielding cover will influence the field distribution and thus the absolute value of the fringing capacitance, but this effect is taken into account by the experimental determination of $C_{\text{fr}}(d_b)$. In a good approximation, changes depend only on the perimeter of the plates and the plate distances and are thus rather independent of the geometric form of the measurement cell.

APPENDIX C
CALCULATION OF THE MEASUREMENT ACCURACY

According to (5) we have $Z = Z_1 + iZ_2 = (t_a/S^{\text{meas}} - 1)/K$ with $K = i\omega C_b(t_a/t_b - 1)$. Since the accuracy of K roughly equals that of the numerator and $K \simeq 1/2Z_0$ (no multiple reflections, see Section III), we will use $Z \simeq (t_a/S^{\text{meas}} - 1)/(2Z_0)$ and multiply the relative error by 2. A calculation [6] according to the error propagation law yields the accuracy as a function of measured amplitude A and phase φ $[t_a/S^{\text{meas}} = A \cdot e^{-i\varphi}]$

$$\Delta_{\text{rel}}|Z| = \frac{4Z_0}{|Z|}\sqrt{\left(\frac{Z_1}{|Z|}+\frac{|Z|}{2Z_0}\right)^2\cdot\left(\frac{\Delta A}{A}\right)^2+\left(\frac{Z_2}{|Z|}\right)^2\cdot(\Delta\varphi)^2}$$

and

$$\Delta_{\text{rel}}\left(\frac{Z_2}{Z_1}\right) = \frac{4Z_0}{Z_1}\sqrt{\left(\frac{\Delta A}{A}\right)^2+\left(\frac{Z_1}{Z_2}+\frac{|Z|^2}{2Z_0Z_2}\right)^2\cdot(\Delta\varphi)^2}.$$

Since the calibration has been taken into account, the absolute accuracy of amplitude and phase measurement is not critical as long as detectors with a good linearity are used. Thus $\Delta_{\text{meas}} = \Delta\varphi \simeq \Delta A/A$ denotes the reproducibility of the phase and amplitude measurement.

For a sample radius of $r = r_c$ holds $Z \simeq Z_p$, $Z \simeq 1/(i\omega C_0\varepsilon)$, and $Z_2/Z_1 = \varepsilon_1/\varepsilon_2$. Thus also $\Delta_{\text{rel}}|\varepsilon| = \Delta_{\text{rel}}|Z|$ and $\Delta_{\text{rel}}(\varepsilon_2/\varepsilon_1) = \Delta_{\text{rel}}(Z_2/Z_1)$ are determined. With $\alpha = 2Z_0\omega C_0$ the above equations become

$$\begin{aligned}\Delta_{\text{rel}}|\varepsilon| &= 2\cdot\Delta_{\text{meas}}\sqrt{(\alpha\varepsilon_2+1)^2+(\alpha\varepsilon_1)^2}\\ &\le 2\cdot\Delta_{\text{meas}}\cdot(1+\alpha\cdot|\varepsilon|)\end{aligned}\tag{15}$$

and

$$\begin{aligned}\Delta_{\text{rel}}\left(\frac{\varepsilon_2}{\varepsilon_1}\right) &= 2\cdot\Delta_{\text{meas}}\cdot\frac{|\varepsilon|^2}{\varepsilon_1\varepsilon_2}\cdot\sqrt{(\alpha\varepsilon_1)^2+(\alpha\varepsilon_2+1)^2}\\ &\le 2\cdot\Delta_{\text{meas}}\cdot\left(\frac{\varepsilon_1}{\varepsilon_2}+\frac{\varepsilon_2}{\varepsilon_1}\right)\cdot(1+\alpha|\varepsilon|).\end{aligned}\tag{16}$$

With modern network analyzers a reproducibility of up to $\Delta_{\text{meas}} = 2.5\cdot10^{-4}$ can be achieved, i.e., a reproducibility of 0.002 dB and 0.014°.

ACKNOWLEDGMENT

The author is very grateful to A. Enders for many valuable discussions.

REFERENCES

[1] J. R. Macdonald, *Impedance Spectroscopy*, 1st ed. New York: Wiley, 1987, ch. 3.
[2] H. J. Eul and B. Schiek, "A generalized theory and new calibration procedures for network analyzer self-calibration," *IEEE Trans. Microwave Theory Tech.*, vol. 39, no. 4, pp. 724–731, 1991.
[3] A. Rost, *Messung dielektrischer Stoffeigenschaften*, 1st ed. Vieweg, 1978, ch. 4.3.
[4] N.-E. Belhadj-Tahar, Ph.D. thesis, Université Pierre et Marie Curie, Paris VI, 1986.
[5] M. N. Afsar, J. R. Birch, and R. N. Clarke, "The measurement of the properties of materials," *Proc. IEEE*, vol. 74, no. 1, pp. 183–199, 1986.
[6] R. Pelster, Ph.D. thesis, Universität zu Köln, 1993.
[7] R. Pelster, German Patent Application P 41 39 622.7, 1991; International Application PCT/EP 92/02711 (1992); and U.S. Patent 5 371 468, Dec. 6, 1994.
[8] H. Freitag, "Einführung in die Zweitortheorie," in *Teubner Studienskripten*, 3rd ed. 1984, ch. 12.
[9] W. J. Getsinger, "The packaged and mounted diode as a microwave circuit," *IEEE Trans. Microwave Theory Tech.*, vol. MTT-14, pp. 58–69, 1966.
[10] ——, "Coupled rectangular bars between parallel plates," *IRE Trans. MTT 10*, pp. 65–72, 1962.
[11] S. F. Adam, *Microwave Theory and Applications*, 1st ed. Prentice-Hall, 1969, ch. 2.2, p. 42.
[12] R. Pelster, P. Marquardt, G. Nimtz, A. Enders, H. Eifert, K. Friedrich, and F. Petzold, "Realization of dielectrics with a metal-like dispersion," *Phys. Rev. B45*, pp. 8929–8933, 1992.
[13] R. Pelster, G. Nimtz, and B. Weßling, "Fully protonated polyaniline: Hopping transport on a mesoscopic scale," *Phys. Rev. B49*, pp. 12718–12723, 1994.
[14] H. Kolodziej and L. Sobczyk, "Investigation of the dielectric properties of potassium hydrogen maleate," *Acta Physica Polonica A39*, pp. 59–69, 1971.
[15] G. Kirchhoff, *Gesammelte Abhandlungen*. Leipzig: J. A. Barth, 1882, p. 112.

Rolf Pelster was born in Leverkusen, Germany, in 1963 and studied physics at the University of Cologne, where he received the diploma degree in 1989 and the Ph.D. degree in 1993.

Since July 1994 he has been a post-doctoral Fellow at the Université Pierre et Marie Curie in Paris, France. His research interests are dielectric and magnetic spectroscopy, mesoscopic 2-phase systems and technical applications (e.g., absorbers), conductivity mechanisms in polymers, water in confined systems, as well as calibration and measurement methods for material test.